



LAWRENCE
LIVERMORE
NATIONAL
LABORATORY

Reduced instability growth with high adiabat ("high foot") implosions at the National Ignition Facility

D. T. Casey, V. A. Smalyuk, K. S. Raman, J. L. Peterson, L. Berzak Hopkins, D. A. Callahan, D. S. Clark, E. L. Dewald, T. R. Dittrich, S. W. Haan, D. E. Hinkel, D. Hoover, O. A. Hurricane, J. J. Kroll, O. L. Landen, A. S. Moore, A. Nikroo, H. Park, B. A. Remington, H. F. Robey, J. R. Rygg, J. D. Salmonson, R. Tommasini, K. Widmann

February 19, 2014

Physical Review E

Disclaimer

This document was prepared as an account of work sponsored by an agency of the United States government. Neither the United States government nor Lawrence Livermore National Security, LLC, nor any of their employees makes any warranty, expressed or implied, or assumes any legal liability or responsibility for the accuracy, completeness, or usefulness of any information, apparatus, product, or process disclosed, or represents that its use would not infringe privately owned rights. Reference herein to any specific commercial product, process, or service by trade name, trademark, manufacturer, or otherwise does not necessarily constitute or imply its endorsement, recommendation, or favoring by the United States government or Lawrence Livermore National Security, LLC. The views and opinions of authors expressed herein do not necessarily state or reflect those of the United States government or Lawrence Livermore National Security, LLC, and shall not be used for advertising or product endorsement purposes.

Reduced instability growth with high adiabat (“high foot”) implosions at the National Ignition Facility

D. T. Casey,¹ V. A. Smalyuk,¹ K. S. Raman,¹ J. L. Peterson,¹ L. Berzak Hopkins,¹ D. A. Callahan,¹ D. S. Clark,¹ E. L. Dewald,¹ T.R. Dittrich,¹ S. W. Haan,¹ D. E. Hinkel,¹ D. Hoover,² O. A. Hurricane,¹ J. J. Kroll,¹ O. L. Landen,¹ A. S. Moore,³ A. Nikroo,² H.-S. Park,¹ B. A. Remington,¹ H. F. Robey,¹ J. R. Rygg,¹ J. D. Salmonson,¹ R. Tommasini,¹ and K. Widmann¹

1) Lawrence Livermore National Laboratory, Livermore, CA 94550

2) General Atomics, San Diego, CA 92121

3) AWE Aldermaston, Reading, Berkshire, RG7 4PR, United Kingdom

Hydrodynamic instabilities can cause pre-existing defects and surface roughness perturbations to grow and degrade implosion performance in ignition experiments at the National Ignition Facility (NIF), resulting in reduced yields. We show here experimental in-flight radiographic measurements of perturbation growth for a low adiabat (“low foot”) versus a higher adiabat (“high foot”) drive. The high foot drive showed distinctly lower perturbation growth, especially for higher mode numbers, opening possibilities for newer, more optimized, ignition designs.

In inertial confinement fusion (ICF) experiments performed at the National Ignition Facility (NIF) [1], capsules containing deuterium-tritium (DT) fuel are imploded to high densities and temperatures with the aim of producing the conditions necessary for thermonuclear ignition [2]. In the indirect-drive scheme, lasers irradiate the inside of a gold hohlraum, producing x rays that then drive a capsule implosion. These x rays heat and ablate the capsule material outward, sending the remaining un-ablated mass, including a shell of cryogenically frozen DT fuel, imploding inward via momentum conservation. The imploding DT shell and remaining ablator then stagnate upon and heat a low density, gas-filled hotspot. In a completely successful ignition experiment, the hotspot will then ignite a burn wave that then continues through the DT shell, producing significant fusion energy and gain. Since the laser ICF concept was first proposed [3], it was recognized that this implosion process is inherently unstable and specifically, reaching ignition is threatened by the Rayleigh-Taylor (RT) instability [4, 5]. Evidence has recently emerged [6-8] that such instability growth, and the resulting mix of ablator material into the hotspot, continues to be a key performance issue for ongoing ignition experiments at the NIF. Ablation front hydrodynamic instability growth is suspected to be one of the dominant sources of this mix. In this letter, we present experimental measurements of ablation front RT growth of pre-imposed single mode surface perturbations. These experiments show that a deliberate modification to the drive to increase the adiabat (α), designed to improve stability [9-11], results in significantly less growth for the most dangerous unstable modes, opening possibilities for newer, more optimized, ignition designs.

During the acceleration phase of the implosion the ablating plasma pushes on the higher density unablated shell, satisfying the unstable condition: $\nabla P \cdot \nabla \rho < 0$ (∇P and $\nabla \rho$ are the pressure and density gradients, respectively), which drives RT growth at the ablation front [12, 13]. This fact has prompted major efforts worldwide to study the RT instability [2, 12, 14-17] and to develop robust ICF ignition designs. This has resulted in substantial developments in both theoretical and experimental understanding of the RT instability (reviewed by several authors such as: [2, 13, 15, 18]). The RT instability grows exponentially in time according to $\eta(t)/\eta_0 \approx e^{\gamma t}$ while in the linear regime ($\eta(t) \lesssim \lambda/2\pi$) [13], where η is a perturbation spatial amplitude, η_0 is the amplitude at $t=0$, and λ is the perturbation wavelength. The growth rate [2, 16] is approximately expressed by:

$$\gamma = a_\gamma \sqrt{\frac{k g}{1 + k L}} - \beta_\gamma k V_a \quad (1)$$

where $k = 2\pi/\lambda$ is the perturbation wavenumber, g is the acceleration, $L = \rho/\nabla\rho$ is the density gradient scale length at the ablation front [16], and V_a is the ablation velocity. Here, a_γ and β_γ are functions of the dimensionless Froude number ($Fr = V_a^2/gL$) and thermal conductivity [16]. Eq. 1 shows that the growth can be stabilized by the ablation process; the stabilizing effects, namely longer gradients and high ablation velocities, are typically associated with reduced compression and lower in-flight aspect ratio (IFAR). Thinner shells can result in higher implosion velocities (for fixed laser energies) and lead to higher predicted 1D performance, but are more vulnerable to ablation front RT growth, as instability can more readily feed-through the thinner in-flight shell, seed growth at other unstable interfaces, and inject mix of ablator material into the hotspot. Much work has been done to make sophisticated target designs that optimize these stability and performance considerations. For example, the ignition target design [19] uses a low adiabat drive (referred to herein as “low foot” drive) to reach high compression, with a plastic CH ablator with roughness requirements designed to mitigate damage from RT growth. Here α can be defined conceptually as the pressure (P) at given density divided by the Fermi degenerate pressure at the same density, or more practically, $\alpha = P/P_{\text{cold}}$ where P_{cold} is the minimum pressure at 1000 g/cc from the DT EOS [19]. The plastic ablator uses a graded high Z dopant (Si or Ge) to shield against high energy x rays so that the ablator density remains higher than or nearly equal to the DT fuel density, $\rho_{\text{ablator}} \gtrsim \rho_{\text{DTfuel}}$, during the acceleration phase to prevent the ablator–fuel interface from becoming classically RT unstable.

Despite the extreme care taken to design targets robust to RT growth, these simulations are extraordinarily complex. They require accurate modeling of initial growth seeds and are sensitive to precision shock timing, x-ray and electron preheat, thermal conductivities, ablator opacities, and the equation of state of the ablator and DT plasmas. Experiments conducted during the National Ignition Campaign (NIC) [8], showed a susceptibility to mix of the ablator into the hot spot beyond that predicted by design simulations. For example, measurements of Ge doped capsule implosions have demonstrated in some cases that ablator material penetrates through the ice layer and into the hotspot in cryogenic implosions [20]. Also, measurements of x-ray yields

relative to neutron yields, in cryogenic DT experiments, have been used to estimate the amount of ablator material that mixes into the hotspot. These data have shown that the magnitude of inferred ablator mass mixed into the hotspot has a strong inverse correlation with the overall yield [7], suggesting that mix is seriously degrading target performance. During the NIC, mix of this magnitude was not predicted in the simulations, which may be due to either uncertainties in our modeling of the instability growth, or in our understanding of the initial perturbations (“seeds”) [7, 21]. For example, artificially increasing the outer-surface roughness in the simulations (3 – 5 \times higher than measured) was able to reproduce most of the performance data [21].

Moreover, recent experiments have demonstrated significantly higher implosion yields and performance much closer to clean 1D predictions [9-11] in implosions with higher entropy in the fuel and ablator. The entropy, or equivalently adiabat (α), was increased by raising the intensity of the initial picket and trough (collectively, the foot) of the laser pulse (see Figure 1a) to create a so called “high foot” drive, utilizing a total of three shocks to precompress the DT shell, compared to the longer four-shock low-foot drive. The corresponding measured radiation temperatures are shown in Figure 1b; both drives reach a peak T_r of 270-280 eV. The higher α from the high-foot drive results in lower compressions (densities) and increased density gradient scale lengths, as shown by simulations using the radiation hydrodynamics code HYDRA [22] shown in Figure 2a. Based on Eq. 1 and the stability discussions above, this should lead to significantly reduced ablation-front RT growth.

To test the hypothesis that the high foot drive significantly reduces ablation-front RT growth, experiments were conducted to directly measure single-mode, linear-regime, ablation-front RT growth for both the low and high foot drives. These experiments used laser pulse shapes (shown in Figure 1a) that were matched to a low foot cryogenic DT shot (~ 350 TW peak power) and a high foot cryogenic DT shot (also ~ 350 TW). The measured hohlraum radiation temperatures, obtained by the Dante diagnostic [23], are shown in Figure 1b. For each increase in the drive temperature (T_R), a shock is launched into the unablated capsule and DT-shell. The high foot drive reaches peak power considerably sooner than low foot due to the faster initial shock launched by the higher foot, since the shock velocity is $\sim T_R^{7/4}$.

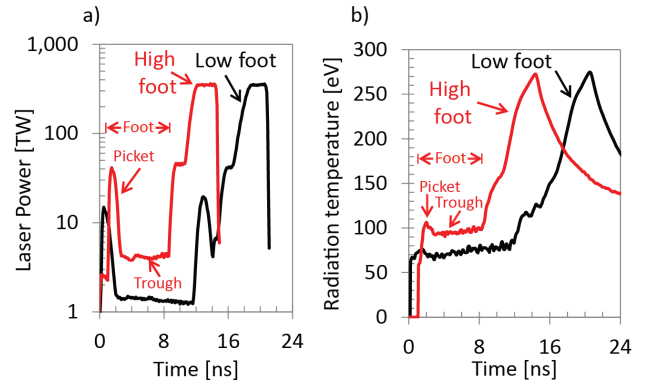


Figure 1: a) Laser pulse shape and b) radiation drive temperature measured on two NIF shots, one shot with the low adiabat (or low foot, black curve) and the other with the high adiabat (or high foot, red curve) drive.

The RT growth rate (Eq. 1) is stabilized by the ablation process through the density gradient scale length and ablation velocity. The ablation velocity is the mass ablation rate (\dot{m}) divided by the ablator density ($V_a = \dot{m}/\rho$) [2]. Reduced compression of the high foot’s higher α ablator (as established during the foot of the drive), in the main acceleration phase, produces a lower ablator density, an increased ablation velocity, and an increased density gradient scale length. The higher α and lower ablator density also results in a longer mean free path for the drive x-rays at the ablation front, which is partly responsible for increasing the ablation front scale length (gentler density slope) [24], as illustrated in Figure 2a with a comparison of the density profiles calculated using HYDRA. The times have been chosen to compare the two density profiles when the DT-fuel / CH-ablator interface is at $650 \mu\text{m}$ for both drives (~ 1.4 times smaller than initial interface radius). The simulated profiles clearly show a longer ablation front scale length, and a lower peak density. This results in a lower inflight aspect ratio by $\sim 1.5 - 2$ for the high foot drive, which enhances stability [9-11].

To quantify these stability differences, Figure 2b shows 2D HYDRA simulations [25] of the outer surface perturbation growth factor, defined as initial over final perturbation amplitude in optical depth (OD). Here, $OD = -\ln(I/I_0) = \int \kappa \delta\rho dR$ where the opacity (κ) is for an x-ray energy of 5.4 keV (the backlighter used in this work, as described below). The perturbation wavelengths are described in terms of Legendre polynomial mode numbers $l = 2\pi R/\lambda = kR$. The simulated growth factor dispersion curves clearly indicate that the high-foot drive is predicted to be less unstable (lower RT growth factors) compared to the low-foot drive.

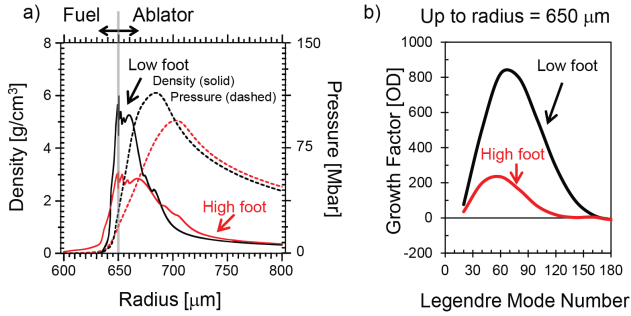


Figure 2: a) Density (solid curves) and pressure (dashed curves) profiles simulated for layered DT implosions using the low foot (black curve) and the high foot (red curve) drives using the code HYDRA [22]. The ablation front is near the point of maximum pressure. The simulated profiles clearly show a longer ablation front scale length, a lower peak density, and a lower inflight aspect ratio for the high foot drive, all properties that enhance stability. b) Simulated optical depth (OD) growth factors for low-foot (black) and high foot (red), plotted as a function of mode number at a radius of 650 μm.

The newly developed hydro-growth radiography platform [25, 26], illustrated by Figure 3, was used to test predictions like those in Figure 2b for the low- and high-foot drives. This platform uses the ignition target design [19] for the hohlraum and the Si-doped CH ablator. The target is similar to actual ignition targets except that the capsule uses a surrogate CH payload to replace the cryogenic DT ice layer and the diagnostic uses a Au cone penetrating one side of the capsule. The capsule has an outer radius of 1120 μm with a total shell thickness of 206 μm. The plastic ablator is doped with three layers of graded Si at 2%, 4%, and 2% atom-%. The inner plastic layer contains a mass-equivalent payload of undoped plastic ~14 μm for a typical cryogenic ice layer (momentum balanced to achieve the same implosion velocity) accounting for the density of CH at 1.06 g/cc (at 32 K) and the solid DT density of 0.255 g/cc (at 20 K). The Au hohlraum is 5.75 mm inner diameter by 9.43 mm tall (inside), with a laser entrance hole 3.1 mm in diameter and is filled with He.

Two capsule types with pre-imposed sinusoidal perturbations were used: one was machined to have an initial perturbation wavelength of 120 μm and 3.4 μm amplitude (peak-to-valley) and another had both 120 μm and 80 μm initial wavelengths, corresponding to $\ell = 60$ and 90, placed side-by-side with amplitudes of 0.5 μm and 0.6 μm, respectively.

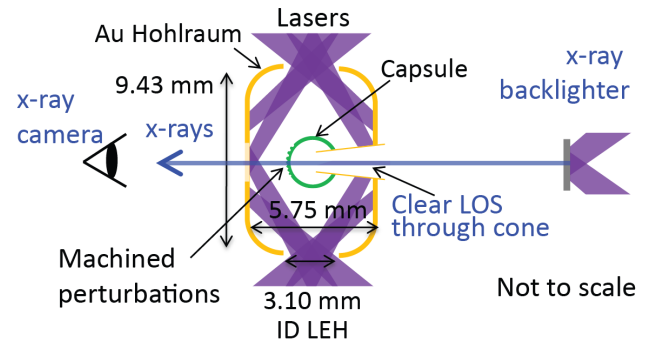


Figure 3: Schematic of indirectly driven hydro-growth radiography target. The capsules are machined with sinusoidal perturbations and backlit using a V foil x-ray backlighter.

A 12.5 μm thick V backlighter [27] is used to radiographically observe the perturbation amplitudes in-flight as a function of time. The V foil is irradiated using eight NIF laser beams focused to an intensity of $\sim 5 \times 10^{14}$ W/cm². In conjunction with x-ray filtering, this produces a nearly monochromatic ~5.4 keV x-ray source from a combination of mostly V He- α and Ly- α that lasts about ~3 ns. The gold cone is attached to the capsule in a similar configuration to the shock-timing “keyhole” platform [28], placed along the imaging axis line-of-sight, to allow single-pass viewing of the perturbation growth through the capsule. The Au cone does not perturb the observed capsule hydrodynamics until times well after the experiments described herein. The backlighter x rays are detected using a gated x-ray camera [29, 30] with 100 ps temporal resolution. The camera is set up with four micro-channel plate strips, providing four time-gated measurements using a 20 μm slit with a resolution of ~20 μm. Since all wavelengths discussed here are $\lesssim 35$ μm all modulations are well resolved [26].

Figure 4a and c show slit image radiographs of modulation growth captured on an x-ray imager using the low foot and high foot pulses, respectively. The images are timed to show the capsule at approximately the same in-flight radii. Distinct differences in contrast are observed due to reduced growth for $\ell = 60$ with the high foot drive. More dramatically, $\ell = 90$ shows very little growth for the high foot drive (consistent with the predictions shown in Figure 2b) because it is near a change in phase (“growth-factor zero-crossing”) due to amplitude oscillation during the Richtmyer–Meshkov (RM) phase, or shock transit phase [31][32], and because the density scale-length and ablative stabilization effects are stronger.

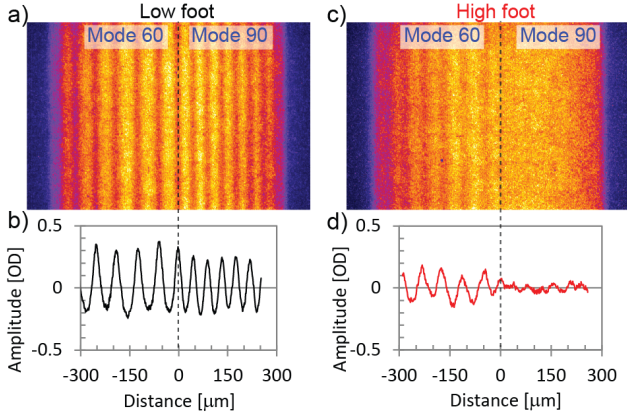


Figure 4: a) Slit image radiograph of side-by-side, pre-imposed, single-mode ripples of $\ell = 60$ and 90 , for the low foot pulse at 20.6 ns, which corresponds to a radius of ~ 613 μm . b) Horizontal line-out in optical depth of the slit image shown in (a). c) Also shown is a slit image radiograph at 14.8 ns, driven with the high foot pulse, which corresponds to a radius of ~ 600 μm for the same side-by-side modes. d) Horizontal line-out in optical depth of the slit image shown in (c).

Figure 5 shows the measured modulation amplitude in OD, obtained using the low foot and high foot drives, during the early phase of the implosion, plotted as a function of wavelength for $\ell = 60$ (Figure 5a and Figure 5b) and $\ell = 90$ (Figure 5c). The fundamental harmonic amplitude is obtained using a Fourier analysis of the central few peaks shown in Figure 4b and Figure 4d. The growth is plotted as a function of the measured wavelength, since the wavelength of the perturbation is directly related to the implosion radial trajectory via: $R(t) = \lambda(t) l / (2\pi)$. The corresponding radius is indicated on the top axis. As the capsule implodes, both the radius and the perturbation wavelength are reduced. The result demonstrates a distinct reduction (~ 2 times smaller) in the growth using the high foot drive at $\ell = 60$ and an order of magnitude smaller growth at $\ell = 90$.

Figure 5 also shows the simulated OD due to instability growth [25], including the diagnostic resolution, compared to the observations. The sources of uncertainty in the growth calculations include uncertainties in the drive and in the initial amplitude as it varies across the imposed perturbation. In particular, the high energy (>1.8 keV), or M-band, portion of the drive is expected to be a dominant source of uncertainty [19], since the mean free path of the drive x-rays determines the ablation front scale length [24] and preheat by the high energy photons affects the density of the unablated CH. However, recent experiments have helped to reduce uncertainties in the drive and spectrum seen by the capsule [33] [34]. The simulations shown in Figure 5 include bands of uncertainty that correspond to $\pm 33\%$ in the M-band fraction, which is an estimate of the remaining growth uncertainty. The comparison shows good agreement between simulation and data and provides a quantitative test of the simulations using these two different drives, at $\ell = 60$ and $\ell = 90$, within this experimental window.

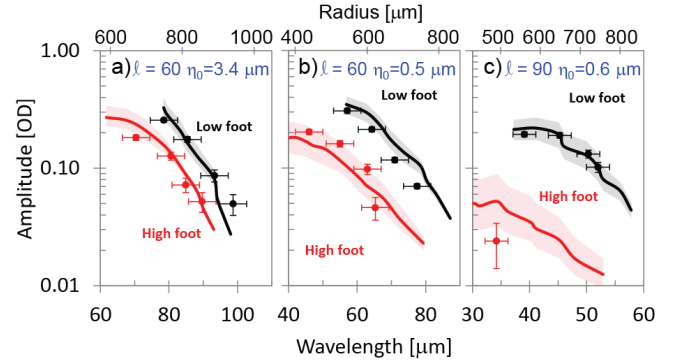


Figure 5: a) Optical depth (OD) modulation amplitude of the fundamental harmonic as a function of wavelength (the top axis shows equivalent radius) for $\ell = 60$ for both the low-foot (black) and high-foot (red) drives observed with 3.4 μm deep (peak-to-valley) modulation initial amplitude. The curves are HYDRA simulations of OD amplitude, while the data are represented by symbols. The shaded bands are included on simulations (solid curves) to illustrate the sensitivity to uncertainties in the drive and the simulation methodology. b) OD amplitude for $\ell = 60$ with 0.5 μm initial amplitudes. c) OD amplitude for $\ell = 90$ with 0.6 μm initial amplitudes.

In summary, a 350 TW high adiabat, or high foot, drive stabilizes hydrodynamic instability when compared to a similar power low adiabat, or low foot, drive. Instability growth calculations do well at reproducing the measured data up to convergence $R_0/R \sim 2$ when the initial seeds are well known. This suggests that unknown seeds, such as perturbations from the capsule support tent [35], may be a significant factor in the performance degradation of the low foot implosions. This picture is supported by recent high resolution 3D Hydra simulations including new models for the tent perturbation that better reproduce the performance of some NIC implosions [36]. It is also possible that growth at other interfaces (e.g. fuel/ablator interface) and at higher convergence could play an important role in reducing implosion performance.

The improved performance of the high foot drives in cryogenic layered DT implosions described elsewhere [9-11], along with the reduced hydrodynamic growth demonstrated herein, underscore the value of mitigating instability growth in NIF ignition experiments. These results will help inform future experiments designed to achieve thermonuclear ignition. More specifically, by raising the foot of the radiation drive, the high foot drive reduced instability growth by shifting the region of positive growth to lower mode number, increasing the ablator density scale length, increasing the ablation velocity, and decreasing the in-flight aspect ratio [37] [9-11].

The authors thank the NIF operations staff who supported this work. This work was performed under the auspices of the U.S. Department of Energy by Lawrence Livermore National Laboratory under Contract DE-AC52-07NA27344.

References

- [1] E. I. Moses, *Journal of Physics: Conference Series* **112**, 012003 (2008).
- [2] J. Lindl, et al., *Physics of Plasmas* **11**, 339 (2004).
- [3] J. Nuckolls *et al.*, *Nature* **239**, 139 (1972).
- [4] L. Rayleigh, *Scientific Papers II* Cambridge, England, 1900).
- [5] G. Taylor, *Proceedings of the Royal Society of London. Series A. Mathematical and Physical Sciences* **201**, 192 (1950).
- [6] S. P. Regan *et al.*, *Physical Review Letters* **111**, 045001 (2013).
- [7] T. Ma *et al.*, *Physical Review Letters* **111**, 085004 (2013).
- [8] M. J. Edwards *et al.*, *Physics of Plasmas* **20**, 070501 (2013).
- [9] O. Hurricane, To be published in *Nature* (2013).
- [10] H. S. Park *et al.*, *Physical Review Letters* **112**, 055001 (2014).
- [11] T. R. Dittrich *et al.*, *Physical Review Letters* **112**, 055002 (2014).
- [12] R. Betti *et al.*, *Physics of Plasmas* **3**, 2122 (1996).
- [13] S. Atzeni, and J. Meyer-ter-Vehn, *The physics of inertial fusion* (Oxford University Press, Oxford, 2004), International series of monographs on physics.
- [14] B. A. Remington *et al.*, *Physical Review Letters* **67**, 3259 (1991).
- [15] J. D.ilkenny *et al.*, *Physics of Plasmas* **1**, 1379 (1994).
- [16] R. Betti *et al.*, *Physics of Plasmas* **5**, 1446 (1998).
- [17] S. G. Glendinning *et al.*, *Physics of Plasmas* **7**, 2033 (2000).
- [18] V. A. Smalyuk, *Phys Scripta* **86**, 058204 (2012).
- [19] S. W. Haan *et al.*, *Physics of Plasmas* **18**, 051001 (2011).
- [20] S. P. Regan *et al.*, *Physics of Plasmas* **19**, 056307 (2012).
- [21] D. S. Clark *et al.*, *Physics of Plasmas* **20**, 056318 (2013).
- [22] M. M. Marinak *et al.*, *Physics of Plasmas* (1994-present) **8**, 2275 (2001).
- [23] E. L. Dewald *et al.*, *Review of Scientific Instruments* **75**, 3759 (2004).
- [24] S. V. Weber *et al.*, *Physics of Plasmas* (1994-present) **1**, 3652 (1994).
- [25] K. S. Raman, To be submitted to *Physics of Plasmas*.
- [26] V. Smalyuk, Submitted to *Phys. Rev. Lett.* (2013).
- [27] C. M. Huntington *et al.*, *Review of Scientific Instruments* **81**, 10E536 (2010).
- [28] H. F. Robey *et al.*, *Physical Review Letters* **108**, 215004 (2012).
- [29] G. A. Kyrala *et al.*, *Review of Scientific Instruments* **81** (2010).
- [30] S. M. Glenn *et al.*, *Review of Scientific Instruments* **83**, 10E519 (2012).
- [31] V. N. Goncharov, *Physical Review Letters* **82**, 2091 (1999).
- [32] L. Peterson *et al.*, to be published.
- [33] S. MacLaren *et al.*, Accepted for publication in *Phys. Rev. Lett.* (2014).
- [34] M. Schneider *et al.*, to be published.
- [35] S. R. Nagel, to be published.
- [36] D. Clark, IFSA 2013 proceedings.
- [37] R. Tommasini *et al.*, to be submitted.